Biophys Rev (2012) 4:323–334
DOI 10.1007/s12551-012-0077-8

REVIEW

Nonlinear optical microscopy in decoding arterial diseases

Alex C.-T. Ko · Andrew Ridsdale · Leila B. Mostaço-Guidolin · Arkady Major · Albert Stolow · Michael G. Sowa

Received: 2 February 2012 / Accepted: 12 April 2012 / Published online: 17 May 2012

Abstract Pathological understanding of arterial diseases is mainly attributable to histological observations based on conventional tissue staining protocols. The emerging development of nonlinear optical microscopy (NLOM), particularly in second-harmonic generation, two-photon excited fluorescence and coherent Raman scattering, provides a new venue to visualize pathological changes in the extracellular matrix caused by atherosclerosis progression. These techniques in general require minimal tissue preparation and offer rapid three-dimensional imaging. The capability of label-free microscopic imaging enables disease impact to be studied directly on the bulk artery tissue, thus minimally perturbing the sample. In this review, we look at recent progress in applications related to arterial disease imaging using various forms of NLOM.

Keywords Atherosclerosis · Nonlinear optical microscopy · Second-harmonic generation · Two-photon excited fluorescence · Coherent anti-Stokes Raman · Artery

A. C.-T. Ko (✉) · M. G. Sowa
National Research Council Canada, Institute for Biodiagnostics,
435 Ellice Avenue,
Winnipeg, Manitoba, Canada R3B 1Y6
e-mail: alex.ko@nrc-cnrc.gc.ca

A. Ridsdale · A. Stolow
National Research Council Canada, Steacie Institute for Molecular Sciences,
100 Sussex Drive,
Ottawa, Ontario, Canada K1A 0R6

L. B. Mostaço-Guidolin · A. Major
Department of Electrical and Computer Engineering,
University of Manitoba,
75A Chancellor's Circle,
Winnipeg, Manitoba, Canada R3T 5V6

Introduction

Arteries, which form a major part of the cardiovascular system, are responsible for the delivery of oxygen and various nutrients to body organs and peripheral tissues to sustain functions of life. Patho-physiological changes within arteries have the potential to severely impact an individual's overall health. The two leading causes of mortality in our societies, myocardial infarction and stroke, are directly linked to arterial disease.

Atherosclerosis, a common arterial disease, is a chronic progressive disease of the arterial intima that is characterized by plaque accumulation on the vessel wall in the large- and medium-sized elastic and muscular arteries. These plaques mainly contain fatty substances, cholesterol, cellular debris, calcium and fibrin. In the past, plaque development was considered to be a passive accumulation of lipids and cellular debris. It is now recognized as a series of highly specific cellular and molecular events that can be described as inflammation-mediated responses resulting from endothelial injury. Structurally, early-stage atherosclerosis manifests through a focal thickening of the endothelium and the formation of localized fatty streaks beneath the endothelium. Fatty streaks can progress to complicated lesions where the accumulation of increasing numbers of macrophages, lymphocytes and extracellular lipid droplets leads to focal necrosis. Continuing progression results in an enlargement and restructuring of the lesion, which is then covered by a collagen-rich fibrous cap overlaying a core of lipid and necrotic tissue (Hansson 2005; Libby 2006), as illustrated in Fig. 1, which shows the anatomy of normal artery wall and atherosclerotic artery wall. When the arterial lumen can no longer dilate to accommodate the growing size of the plaque, blood flow becomes impaired, leading to ischemic pain and eventually more serious consequences. Such stenotic lesions tend to develop slowly, preceded by a number of warning signs

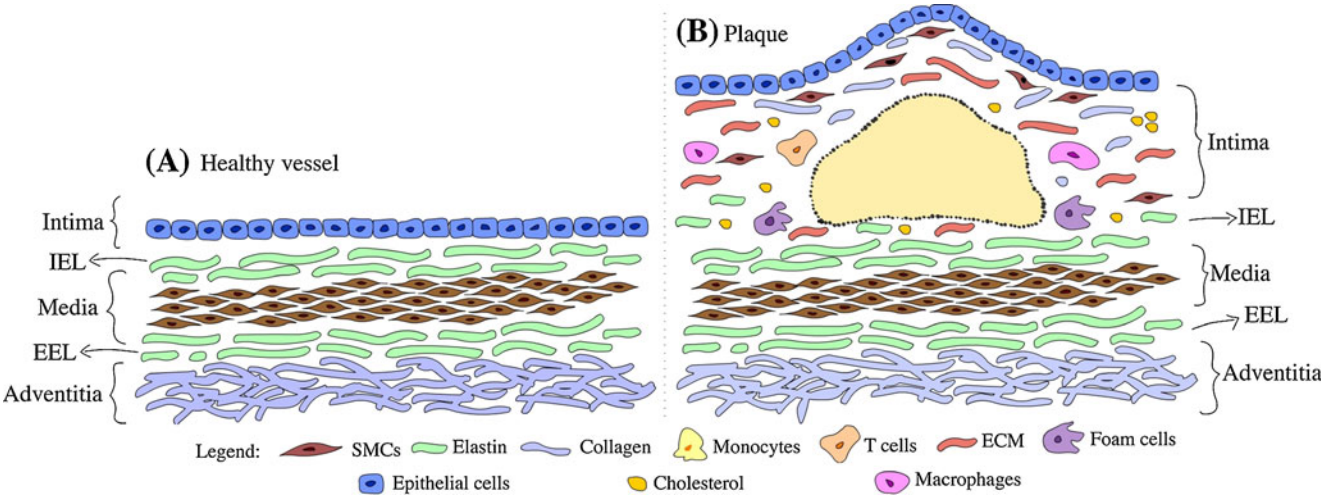

Fig. 1 **a** Typical anatomy of a healthy artery wall showing three distinct pathological layers, i.e. intima, media and adventitia, each separated by internal elastic lamina (*IEL*) and external elastic lamina (*EEL*). **b** Atherosclerotic plaque, IEL is partially broken with no clear boundary between the lesion body and the media layer. *SMC*, Smooth muscle cells, *ECM* extracellular matrix

prompting intervention. Conversely, in unstable lesions the fibrous cap can rupture or erode with little or no clinical warning, resulting in the ejection of the lipid core into the vessel, i.e. causing a clot or thrombosis. This usually impedes blood flow in the artery, leading to a serious, often life-threatening, ischemic event. Even without thrombosis, hardened and narrowed arteries as a result of atherosclerotic plaque build-up can still cause reduced blood flow to organs and other parts of body, giving rise to serious health conditions.

Most clinical imaging techniques have been applied to detect blockages in blood flow and locate narrowed sections of vessels and as such, they are suited to detecting stenotic lesions and aid in the management of patients with acute blockages. Intravascular ultrasound (IVUS) and more recently optical coherence tomography are imaging technologies that are available to clinicians to visualize plaque structure in the vessel wall (Hodgson et al. 1993; Yock and Fitzgerald 1998; Jang et al. 2005; Barlis et al. 2008a, b; Sun et al. 2008; Barlis and Schmitt 2009). Recent studies have shown the potential of fluorescence lifetime imaging to differentiate thin plaques from thick plaques and thick-cap fibroatheroma based on UV-excited fluorescence lifetime data (Suhling et al. 2005; Jo et al. 2006; Marcu et al. 2009; Phipps et al. 2009; Thomas et al. 2010). However, none of these methods are able to resolve the composition of individual plaques nor can they detect early compositional changes within atherosclerotic intima. Studies have shown that both the morphology and composition of plaques are crucial for understanding their development and predicting the risk of plaque rupture or erosion. In fact, the risk of rupture in non-stenotic plaques is more influenced by plaque composition than by morphological features (Naghavi et al. 2003).

Despite recent advances in imaging technologies, histological examination remains the standard for clinical diagnosis. Compared to most imaging techniques, histology provides compositional information of the plaque in a structural context even though the fixation process can result in alterations in extracellular arrangement. An emerging optical method, nonlinear optical microscopy (NLOM), can provide micron-scale compositional data while preserving the structural context. In this review, we discuss the latest developments in NLOM techniques for arterial imaging and their potential role as an adjunct to histology studies in vascular biology and possibly clinical vascular pathology.

The technology: nonlinear optical microscopy and hardware requirements

Nonlinear optics (NLO) is a branch of optics that describes the nonlinear interaction of light with media. In NLO, the dielectric polarization of the medium responds nonlinearly to the electric field of the light. There are a number of possible NLO responses in tissue that could give rise to image contrast. The best known of these are two-photon excited fluorescence (TPEF) (Denk et al. 1990), second-harmonic generation (SHG) (Sheppard et al. 1977) and coherent Raman processes, such as coherent anti-Stokes Raman scattering (CARS) (Duncan et al. 1982; Zumbusch et al. 1999). Figure 2 shows an energy diagram illustrating the TPEF, SHG and CARS processes. Other NLO processes that have been demonstrated to generate useful image contrast include third-harmonic generation (Barad et al. 1997), sum-frequency generation (Mizutani et al. 2005), resonance-enhanced four-wave mixing and stimulated coherent Raman scattering (Freudiger et al. 2008). Since several nonlinear processes can be simultaneously excited in the focal spot, multi-contrast imaging microscopes with parallel detection

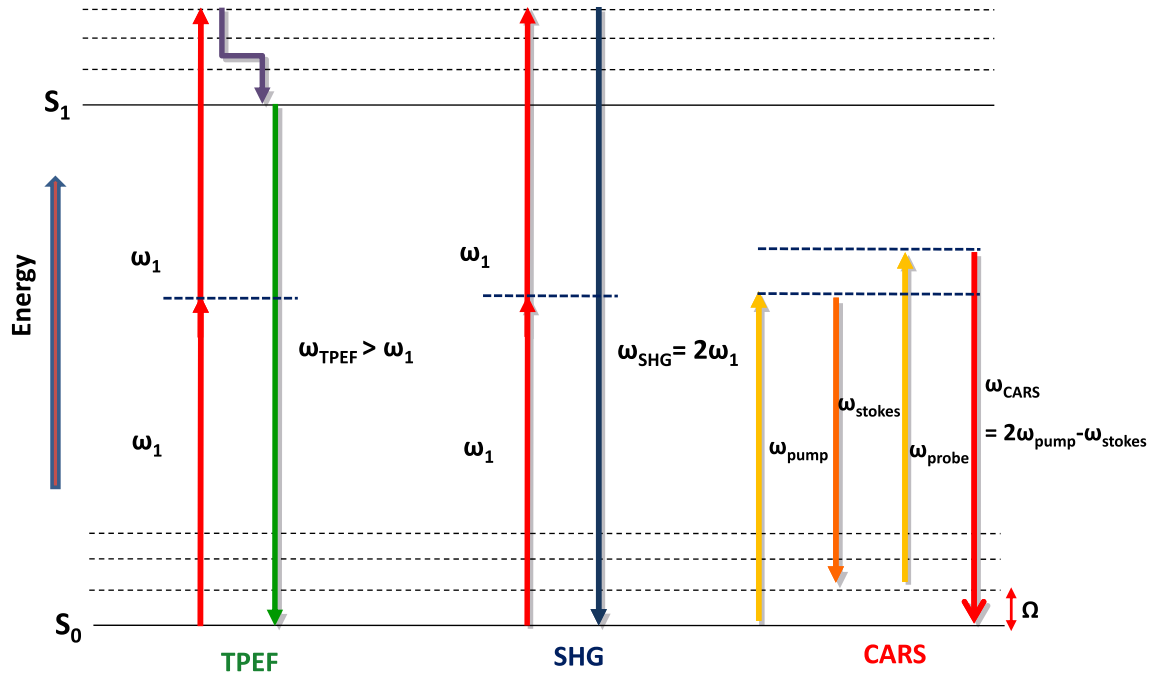

Fig. 2 An energy diagram illustrating three best known nonlinear optical (NLO) processes used in biomedical imaging: two-photon excited fluorescence (*TPEF*), second-harmonic generation (*SHG*) and coherent anti-Stokes Raman scattering (*CARS*)

channels are often implemented, adding to the versatility of NLOM to study the structure and chemical composition of biological samples.

Under normal light conditions the probability of NLO processes is negligible, but they can become significant at high electric field strengths of a temporally and spatially focused light beam. To achieve the necessary high transient intensities without destroying the sample, ultrafast pulsed laser excitation on femtosecond and picosecond scales is widely used.

Laser sources

The generation of NLO signals typically requires the use of a mode-locked ultrafast pulsed laser, such as the titanium-ion-doped sapphire (Ti:sapphire) laser (Spence et al. 1991). It is usually configured to operate at about 80 MHz of repetition rate, producing pulses around 100 fs in duration, and with an average output power in the range of a few hundred mW to 2 W. The output wavelength can be tuned from about 700 to 1000 nm, with peak operating output power at 800 nm, a wavelength well suited for imaging atherosclerotic plaques using endogenous contrast.

In addition to the conventional Ti:sapphire lasers, high-power, ultrashort pulse bulk solid-state or fiber lasers are now available commercially and are frequently used for nonlinear microscopic imaging (Millard et al. 1999; Prent et al. 2008; Pegoraro et al. 2009a, b). Most commonly, Er^{3+} (1540 nm) or Yb^{3+} (1030 nm) doped glasses make up the core of these fibers (or bulk crystals) and constitute the gain medium. Pulse energies in the range of 1–10 nJ at repetition rates of 10s of MHz are readily available. These lasers can be frequency doubled to achieve the operation of Erbium-based systems at around 780 nm (Miyata et al. 2009) and of Ytterbium systems at around 515 nm (Major et al. 2009). Monolithic all-fiber designs have also been implemented. Delivery of sub-ps pulses at the tip of a fiber is an important advantage of endo-microscopy applications.

Coherent Raman microscopy, such as CARS and stimulated Raman scattering (SRS), requires the mixing of two precise frequencies of light where the frequency difference matches a frequency of a vibrational mode of the molecules in the sample. Therefore, the frequency difference between the two incident wavelengths, the pump and the Stokes, can be used for selective elucidation of the molecular origin of the produced coherent Raman signal. In CARS, a third color (probe frequency) is scattered at a higher (anti-Stokes) frequency, gaining energy equivalent to the Raman mode (see Fig. 2). For most implementations of CARS microscopy, this probe frequency is identical to the pump frequency. In multi-modal imaging, TPEF, SHG and CARS signals can be easily separated by optical filtering (Ko et al. 2010).

There are two fundamental distinctions between laser sources for coherent Raman microscopy where at least two pulsed laser beams should be synchronized in time and overlapped in space. The first is between broadband (approx. 100 fs or 200 cm^{-1} of bandwidth) and narrowband (>1 ps and around 20 cm^{-1} bandwidth) sources. The second difference is between

single cavity configurations where additional frequencies are generated outside the cavity, or where cavities are locked together. The initial implementations of CARS microscopy employed two synchronized ps Ti:sapphire oscillators. Although longer pulses require higher average powers to achieve the same nonlinear optical signal compared to using shorter pulses, the narrow bandwidths of ps pulses better match the typical Raman mode line-width of approximately 10 cm^{-1}, thus providing better spectral resolution. In the case of imaging condensed lipid material where the effective bandwidth of the C–H resonance is closer to 200 cm^{-1}, fs pulses are sufficient to provide a reasonable contrast (Rinia et al. 2008). Utilizing two independent Ti:sapphire oscillators requires electronic synchronization; however, fluctuations in cavity length can give rise to a time jitter that can cause the system to drift out of synchrony. This problem can be solved by using one oscillator slaved to the other such that slight adjustments in its cavity length can keep the systems running synchronously. One advantage to using two-oscillators system is its frequency tunability to cover the entire Raman shift region. Power and stability suffer as the frequency difference is increased.

An alternative for the generation of the second color beam (e.g. Stokes) involves the use of the output with only a single oscillator. There are various strategies for this approach: (1) using an optical parametric oscillator (OPO) (Ganikhanov et al. 2006); (2) mixing the frequencies from a single high bandwidth pulse (Dudovich et al. 2002); (3) generating new spectral components using a photonic crystal fiber (PCF) (Paulsen et al. 2003). Figure 3 illustrates simplified configurations of OPO- and PCF-based multimodal CARS systems. In each case the pump and Stokes pulses are generated from the same seed pulse and so do not suffer from inter-pulse time jitter. Note that OPOs also require additional cavity-stabilization electronics similar to those found in locked oscillators.

The earliest implementations of CARS microscopy using PCFs were in the so-called multiplex CARS configuration where the dispersed CARS spectrum over a few hundred wave-numbers was detected by a spectrometer. PCF with two zero-dispersion wavelengths (ZDW) can have very low noise levels similar to the oscillators used to pump them (Murugkar et al. 2007). This type of two-ZDW PCF is commercially available and targeted specifically for CARS microscopy. It has a low noise and good spectral-power density of around 1000–1200 nm to mix with the T:sapphire pump for imaging of lipids with an anti-Stokes signal of around 650 nm. Moreover, the PCF output can be chirp matched to the pump for spectral focusing (Pegoraro et al. 2009a, b). Good resolution hyper-spectral CARS imaging can be carried out across the approximately 1700 cm^{-1} of bandwidth of the Stokes pulse.

Microscope

The dominant form of NLO microscopy is laser scanning imaging, and in this approach a collimated laser beam is expanded to fill the back pupil of the objective lens positioned to produce a diffraction-limited spot. Changes in the angle of the beam entering the lens result in the translation of the focused light in the image plane. The focus is raster-scanned in the sample, and the signal is detected by a fast-responding detector, such as a photomultiplier tube (PMT). The image is built up pixel-by-pixel under software control where the positioning of the scanned beam is synchronized with the incoming signal from the detector. As the signal is restricted to the regions of the highest light intensity, i.e. at the focus, NLOM provides optical sectioning where in-focus images at different depths within the sample can be generated. Many confocal laser scanning microscopes (LSM) can be adapted with minimal modification for NLOM by bringing the ultrafast laser beam through the appropriate path. There has been extensive research and development in miniaturized fiber-based confocal LSMs where both excitation laser and detected signal propagate through flexible fiber assemblies. These include commercial devices for both research and clinical endomicroscopy (Delaney and Harris 2006). The adoption of similar devices for NLO contrast, however, presents additional challenges due to the added requirements of effective transmission of pulsed laser light in fiber.

Arterial and atherosclerotic tissue imaging

TPEF and SHG imaging

The mechanical properties of blood vessels are modulated by vessel wall components, such as collagen fibrils and elastin fibers. The micro-architecture of these structural proteins within the different layers of the arterial wall, intima, media and adventitia determines the strength and flexibility of the blood vessel. Selective imaging of collagen and elastin is therefore of interest in understanding fundamental arterial tissue mechanics and biochemistry. Extracellular elastin has been shown to have significant two-photon-excited autofluorescence. Collagen, in particular type-I collagen fibrils, along with myofibrils and tendon are efficient SHG centers in biological tissues. Combined TPEF/SHG thus allows for co-localized selective imaging of elastin and collagen organization in the arterial wall without additional labeling. This label-free approach can better preserve tissue structural integrity, thereby providing more reliable structural and compositional information. As illustrated in Fig. 4, the TPEF image of an ethanol-fixed atherosclerotic artery section clearly reveals a different extracellular matrix (ECM) morphology compared to an unfixed section, indicating structural alteration upon fixation.

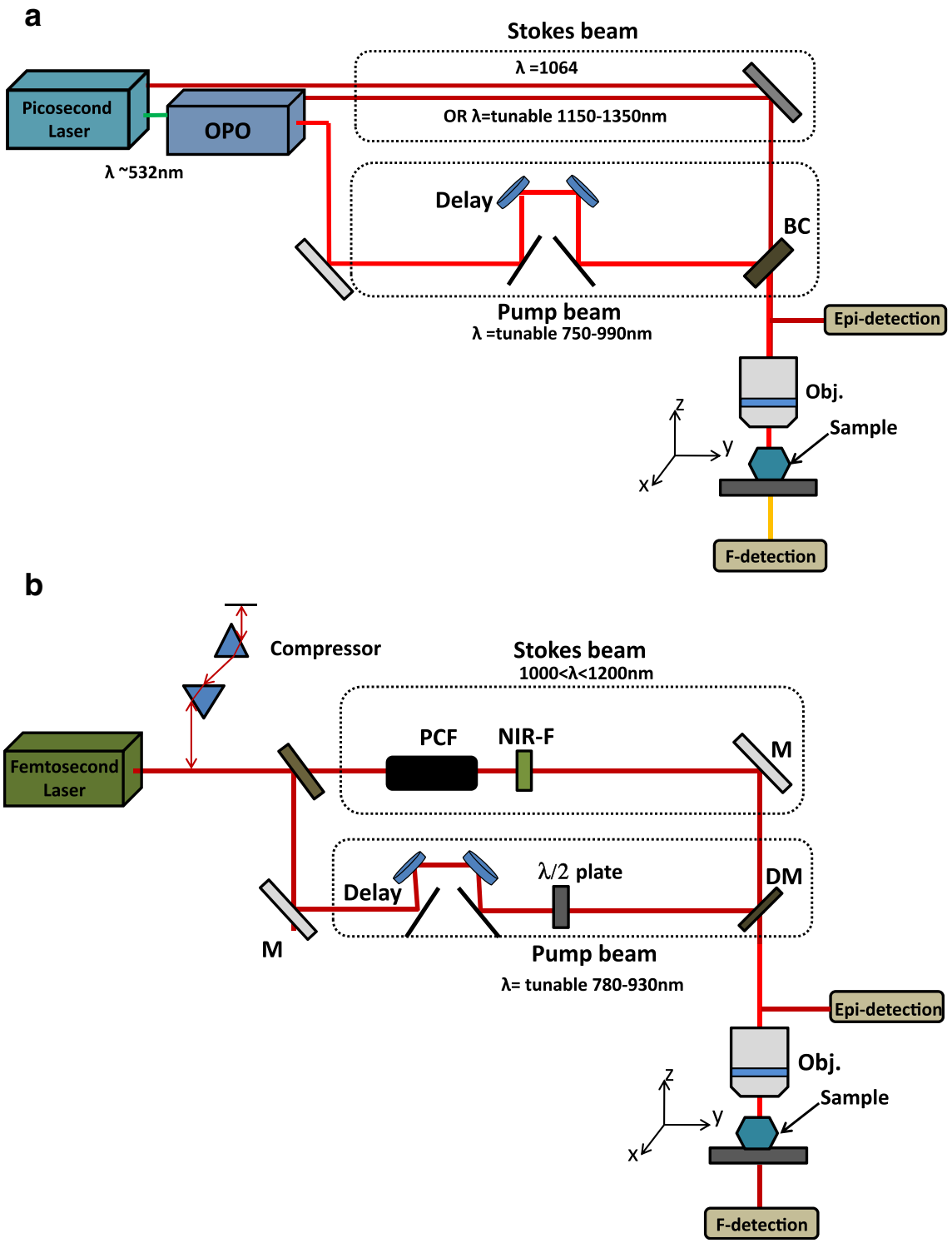

Fig. 3 Schematic illustration of two common configurations of multimodal NLO microscopes. Each can provide contrast from SHG, TPEF and CARS. **a** Picosecond system with optical parametric oscillator (*OPO*). **b** Femtosecond system where the Stokes beam is generated in a photonic crystal fiber (*PCF*)

Simultaneous selective collagen and elastin imaging of the vessel wall can be achieved by monitoring two emission wavelength regions through optical filtering. With 800-nm laser excitation, a sharp SHG band can be typically detected at 400±5 nm and a boardband TPEF peaks at around 500 nm, as illustrated in Fig. 5. The small but sharper SHG emission represents collagen, and the broad TPEF band can be mainly attributed to elastin, or more precisely

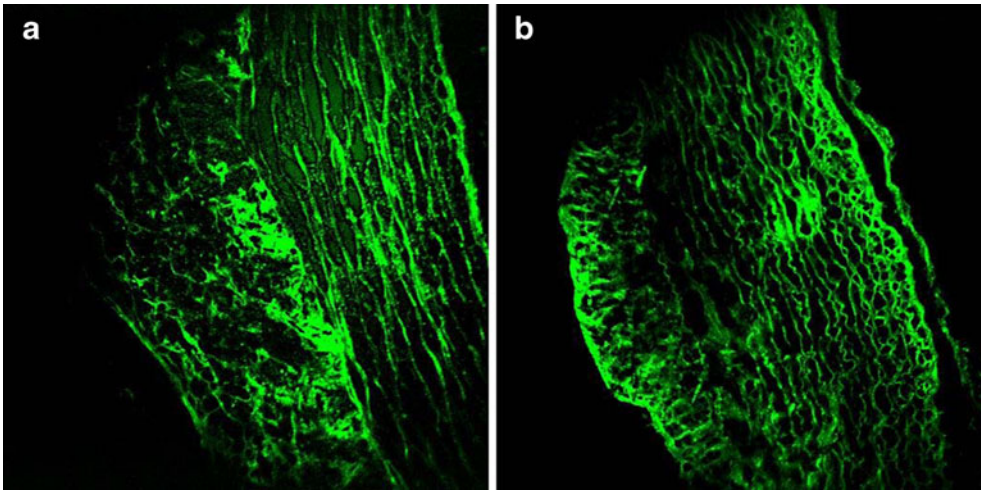

Fig. 4 TPEF image of a 95 % ethanol-fixed, unstained, rabbit's artery cryosection (**a**) and an unfixed, unstained rabbit's artery cryosection (**b**). Marked differences are observed in the structure of the elastic fibers located within the tunica media layer

to the covalent cross-links (iso/desmosine) found in elastin. The well-separated TPEF and SHG bands allow effective visualization of collagen and elastin micro-structures with minimum cross-talk.

NLOM imaging of arteries has been reported using different instrumental configurations and different animal models. Parasassi et al. (2000) first used TPEF to study aorta fibers proteolysis induced by low-density lipoprotein (LDL) hydroperoxides. Using freshly cross-sectioned arteries from ApoE−/− mice, they imaged the activation of a redox-sensitive proteolytic process in the arterial wall triggered by lipid hydroperoxides in LDL. Curved and damaged extracellular protein fibers were observed after incubation of the aorta with either LDL containing lipid hydroperoxides, or tert-butyl-hydroperoxide. Later, Zoumi et al. (2004) reported the first comprehensive ex vivo imaging study of artery microstructure using combined TPEF/SHG microscopy with biochemical specificity. Thin sections of rabbit artery were examined using two-photon LSM. Co-registered collagen and elastin microscopic images were acquired at different locations on transverse-sectioned artery samples from the intima to the adventitia. Multiphoton emission spectra acquired at the tunica adventitia and the tunica media showed a marked difference in SHG band intensity, indicating different collagen density at the various layers of the artery wall. In a rat study, Boulesteix et al. (2005) validated unstained TPEF/SHG images of transverse sections of artery with histological sections. They also performed the first en face imaging of the artery lumen of bulk tissue by directly visualizing the extracellular features of the vessel wall. The internal elastic lamina (approx. thickness <5 μm) on the carotid arterial lumen was resolved through TPEF using a high numerical aperture water-immersion objective lens. Multiple band-shaped elastic lamina and occasional fenestrations in the lamina were visible. A bovine study by Schenke-Layland et al. (2005, 2006) examined the morphology of the ECMs of cardiovascular structures using three-dimensional NLOM. A distinct structure of the elastic fibers at the inflow side and dense bundled collagenous structures at the outflow side of ovine aortic and pulmonary heart valve leafsets were observed.

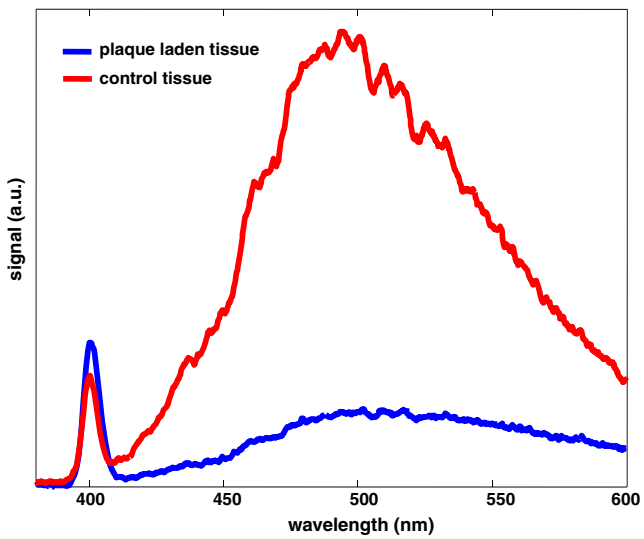

Fig. 5 Representative two-photon emission spectra of a healthy and atherosclerotic artery lumen, respectively, at an excitation at 800 nm. The *smaller/sharper* band centered at 400 nm is SHG (collagen type-I) and the *broader* emission band centered around 500 nm is TPEF (elastin/other macromolecules, such as foam cells and macrophages). Note the dramatic different SHG/TPEF ratios between healthy and plaque-laden lumen

Van Zandvoort et al. (2004) imaged sections of the atherosclerotic vascular wall using NLO–LSM. On lesions developed in ApoE−/− mice, they observed abundant collagen fibrils in the adventitia, media, plaque core and fibrous cap using SHG, while elastin bands were only present in the media, as evident from the strong green TPEF. Labeled cell nuclei (e.g. smooth muscle cells and macrophages) with vital DNA/RNA stain Syto13 were also found to emit strong two-photon fluorescence at slightly different wavelengths from that of elastin. This approach enabled the simultaneous

imaging of elastin, collagen and cell nuclei on a single-stained (e.g. nucleic acid dyes) slice. Common plaque components, such as macrophages or extracellular lipids, did not show significant intrinsic NLO emissions. Both necrotic core and extracellular fat deposits were weakly fluorescent. In another study of vital murine elastic and muscular arteries, Megens et al. (2007) were able to detect differences in structural vessel wall components between elastic and muscular arteries using TPEF imaging. In particular, differences in the sizes and density of internal lamina fenestrae, smooth muscle cells, number of elastic laminaes and adventitial collagen structure were detected. A correlation between inflammatory cell activity and increased collagen in activated endothelia was also observed (Megens et al. 2008) . More recently, these authors demonstrated in vivo imaging of the arteries of small rodents using fluorescence-tagged TPEF based on accelerated image acquisition triggered on cardiac and respiratory activity. Megens et al. (2008) and Doras et al. (2011) investigated the changes in collagen structure inside an artery wall affected by atherosclerosis using reconstructions of multiphoton images as well as optical polarization state analysis. Using excised human aortas, Lilledahl et al. (2007) demonstrated combined TPEF and SHG imaging of fibrous caps to predict plaque vulnerability. This work showed en face NLOM imaging of plaque to a depth beyond 65 μm from the lumen face through the fibrous cap in thin-capped fibroatheroma and into the lesion core, clearly demonstrating the potential of NLOM to differentiate between vulnerable and stable plaques. Yu et al. (2007) also studied atherosclerotic plaques in ApoE−/− mice using in vivo TPEF/SHG imaging and reported en face imaging of the accumulation of enhanced green fluorescent protein expressed by leucocytes on the lumen face. This study revealed a stimulated focal accumulation of leukocytes triggered by acutely overstretching the artery, a typical lumen injury that can initiate plaque formation. Maffia et al. (2007) studied the immune response to vascular damage in an effort to understand lymphocyte responses in the lamina adventitia and its role in atherosclerosis development. Different from conventional analysis systems, such as flow cytometry, and immunohistochemistry, NLOM provides a unique window to observe these events without physical/chemical disruptions to the tissues. Maffia et al. (2007) reported a three-dimensional imaging of the entire structure of an isolated intact ApoE−/− mouse carotid artery, identifying a homed, fluorescently tagged, adoptively transferred lymphocytes.

Based on a measure of the collagen to elastin density ratio (or SHG:TPEF intensity ratio), Lilledahl et al (2007) and Smith et al (2009) developed an approach to detect vulnerable plaques based on the assumption of a higher collagen density in atherosclerosis lesions, especially in fibroatheroma, compared to the normal vessel wall. Using histological specimens as a reference, Lilledahl et al (2007) reported a specificity of 81 % in detecting fibrous cap atheroma using collagen to elastin ratios derived from pixel-based image quantification. In contrast, Smith et al (2009) reported an approach based on two-photon spectroscopic data. Marked changes in two-photon spectra were observed at the sites of atherosclerotic lesions. The marked increase in the SHG:TPEF band intensity ratio provided the contrast for detecting plaques (Fig. 5). In another study, Timmins et al. (2010) used sub-10-fs pulses generated by TPEF/SHG to examine the orientation of fibrillar collagen and elastin fibers in the inner medial region of bovine carotid arteries upon mechanical loading. The results of this investigation added to our knowledge of the complex structure–function relationships in vascular tissue, leading to a better understanding of the patho-physiological processes resulting from injury, disease progression and interventional therapies.

CARS-based multimodal imaging

Lipids play a central role in the pathogenesis of artherscleorosis, but lipids generate little intrinsic SHG or TPEF emission. Adding CARS to the existing combination of TPEF/SHG provides a means to specifically image lipids concurrently with the key structural proteins, elastin and collagen.

Traditional techniques, such as immunohistochemistry and lipid extraction measurements, are the standard methods used to study lipid biology. However, these methods either require destructive measures or lack the power to resolve spatial information to understand lipid function. As alternatives, CARS and third-harmonic generation (THG) are effective in lipid imaging. CARS microscopy, a chemical imaging method using molecular vibrational modes as contrast, is particularly suited for imaging lipid-rich structures which have high-density CH_2 groups. In principle, CARS could be used to image many different biological components; in practice, it has found its most successful applications in lipid imaging due to the abundance of lipids in cells, organs and tissues, combined with the strong Raman cross-section of the C–H stretching vibrations.

There are many reports of using CARS to image arteries. Le et al. (2007) reported multimodal CARS imaging of atherosclerotic lesions in arteries from a swine model of metabolic syndrome-induced arterial disease. In this study, CARS imaging was performed with two tightly synchronized Ti:sapphire lasers operated with picosecond pulses, while the SHG/TPEF imaging was carried out with a third femtosecond laser operated at 800 nm. A number of important cellular and extracellular components, including endothelial cells, extracellular lipids and foam cells, in the plaque-affected area were visualized without the need to stain the tissue by viewing the luminal side of the vessel wall. By comparing co-localized TPEF and CARS images of the same lesion, Le et al. (2007) were able to differentiate

oxidized low-density lipoprotein (LDL) aggregates from cholesterol-rich LDL particles and neutral lipid droplets. In addition to imaging lipid structures, Le et al. (2007) also observed altered collagen fibril morphology in lesions using SHG imaging. The healthy lumen showed an organized collagen fibril structure exhibiting an almost parallel alignment to one another. Lesions, however, showed a disoriented collagen fibril morphology with the collagen fibrils in the atheroma running perpendicular to those within the artery wall. A study by Wang et al. (2009) focused on imaging arterial cells in relation to the extracellular matrix using a similar multimodal CARS microscope with ps laser pulses, not fs pulses, for TPEF and SHG generation. Using two mode-locked ps Ti:sapphire lasers (one master and one slave), Wang et al. (2009) obtained high-resolution images of the normal artery wall at various depths from the lumen. CARS imaging was able to resolve the luminal endothelium monolayer based on the signal originating from the endothelial cell membrane. The internal elastic lamina (IEL) was also revealed at a slightly deeper layer based on elastin TPEF emission. In addition to autofluorescence, the elastic membrane also showed a CARS signal. In contrast to the typical CARS signal originating from an ordered orientation of CH_2 groups in lipid bilayers, the CARS signal from IEL was found to be polarization independent and thought to come from disordered orientation of CH_2-rich residues in the cross-linking region. Without seeing visible thermal damage to artery tissue, Wang et al. (2009) concluded that ps laser was a feasible light source to use for SHG/TPEF generation in arterial tissue despite the requirement of a higher average power compared to femtosecond sources.

Using an innovative photonic crystal fiber-powered multimodal CARS microscope with fs pulses, Ko et al. (2010) reported en face visualization of atherosclerotic plaque development in a myocardial infarction-prone rabbit model. Structurally similar to swine arteries, healthy rabbit artery also presents a distinct layer of IEL located near the lumen surface that can be visualized through TPEF (Fig. 6a). The morphology of this IEL layer resembles that in swine artery observed by Wang et al. (2009). At a deeper layer (approximately 20 μm), a different fibril structure emerged with an orientation nearly perpendicular to that of IEL membrane (Fig. 6b). This fibril structure was believed to be the bulk elastin network in the arterial tunica media. In NLOM images of atherosclerotic lesions, the IEL is no longer clearly visible, and scattered collagen fibrils, an accumulation of lipid-rich structures and nonfibrous fluorescent structures dominate the image (Fig. 7). Advanced plaque showed a different collagen fibril morphology and presented a denser system of nonfibrous fluorescent structures. Ko et al. (2010) reported the first depth scan images of rupture-prone plaques. Figure 8 shows a typical thin collagen cap overlaying a lipid-rich core at approximately 50 μm below the fibrous cap.

Kim et al. (2010) recently presented the first en face multimodal CARS imaging study that demonstrated increased lipid accumulation in the arteries as a result of dietary conditions. In this study, several cellular and structural features of early stage Type II/III atherosclerotic plaques in ApoE−/−mice were characterized, specifically the infiltration of lipid-rich macrophages and the structural reorganization of collagen and elastin fibers in thick tissue specimens. In another recent study, Wang et al. (2011) interrogated stented coronary arteries of swine under different diet regimens and stent deployment conditions. Changes in arterial structure and composition after stenting were inspected by multimodal CARS microscopic imaging. These authors were the first to use multimodal CARS to image cellular proliferation, lipid accumulation and extracellular matrix changes in the arterial media and neointima after stent deployment. The major findings of this study include stellate-shaped cells observed in CARS images in association with classical neointimal hyperplasia in the stenotic, in-stent segments of the artery. The study also clearly showed the proliferation of smooth muscle cells in these areas.

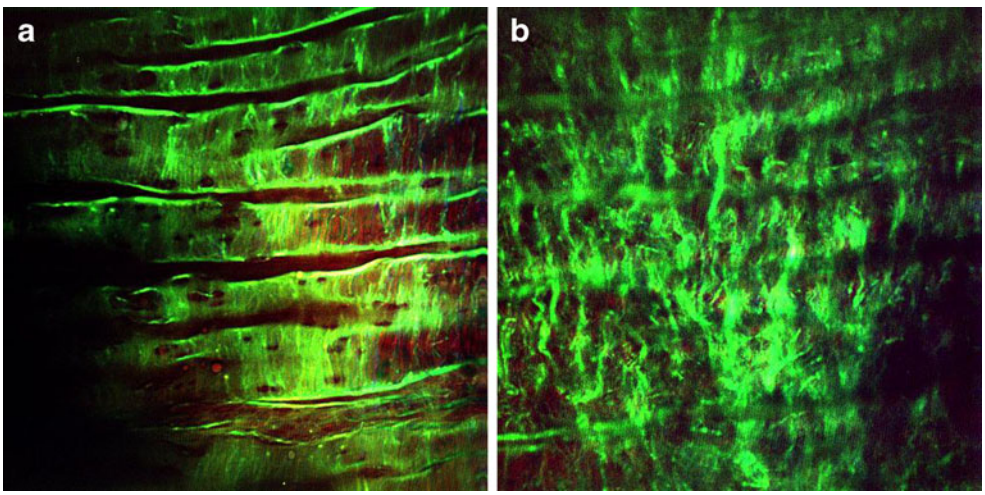

Fig. 6 En face NLOM images of the healthy artery lumen showing the IEL (**a**) and the elastic fiber network underneath the IEL (**b**). The imaging plane is approx. 50 μm below lumen surface (within tunica media)

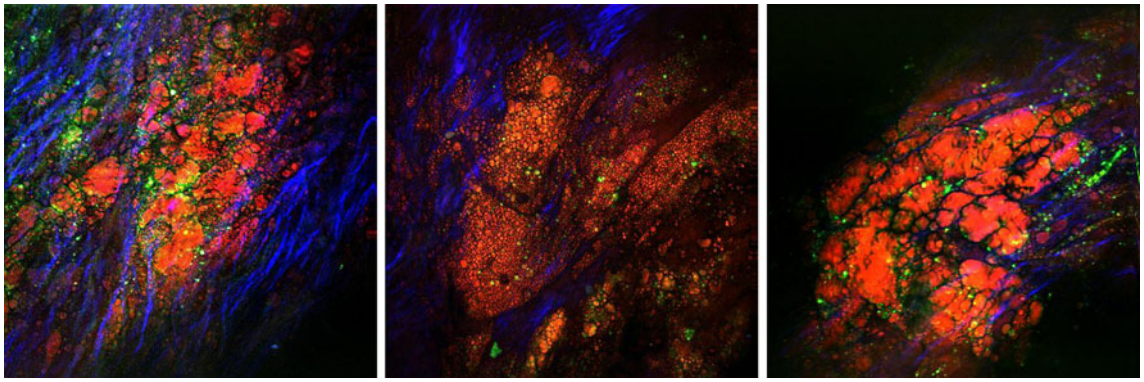

Fig. 7 En face NLOM images of atherosclerotic lesions. *Red/orange* CARS illustrating lipid-laden structures, *green* TPEF illustrating fluorescent macromolecules (e.g. oxidized low-density lipoprotein), *blue* SHG illustrating fibrillar collagen type-I

SHG analysis indicated that collagen content was lower in the neointima than in the arterial media and even lower in those segments where a drug eluting stent was deployed .

Broadband CARS imaging

To date, most imaging CARS studies have used a single C–H stretching vibrational mode as a source of contrast (approx. 2845 cm^{-1}) to provide fast vibrational imaging of lipid-laden structures. However, in order to obtain added CARS spectral contrast using two narrow-band laser sources, the Raman shift has to be tuned, and this approach is slow. Recently, Lee et al. (2009a three-color (three-laser) multiplex CARS for fast imaging and microspectroscopy over the entire CH stretching vibrational region. In this study, narrowband Stokes (approx. 3.5 cm^{-1}) and probe (approx. 5 cm^{-1}) beams were overlapped with a broadband (450 cm^{-1}) pump beam to generate CARS spectra covering the entire CH stretching vibrations (approx. 2600–3100 cm^{-1}). Kim et al. (2010) performed a multiplex CARS spectroscopic study to investigate the distinct chemical profiles of various atherosclerotic lipids based on the same broadband CARS platform. Clear spectral differences were detected among four different types of lipid morphology observed in ApoE−/− mice arteries: plate-shaped lipid crystal, needle-shaped lipid crystal, extracellular lipid deposits and lipid-laden form cells. Using multiplex CARS, these authors also reported that changes in the chemical profiles of lipid crystals occurred due to statin therapy. Attenuated peaks were observed at 2870, 2910 and 2950 cm^{-1}, which were attributed to lipid phase changes and changes in protein content.

Pegoraro et al. (2009b) recently demonstrated a novel spectral focusing implementation to acquire high resolution CARS spectra in the C–-H stretching vibration region, using an optimally chirped multimodal CARS microscopy based on a single femtosecond Ti:sapphire laser and synchronized PCF output. Preliminary data showed that clear spectral differences could be detected from multiple regions of interest identified in a rabbit artery section.

Quantitative image analysis

In order to become a truly useful imaging tool, NLOM should move beyond phenomenological studies. The visual

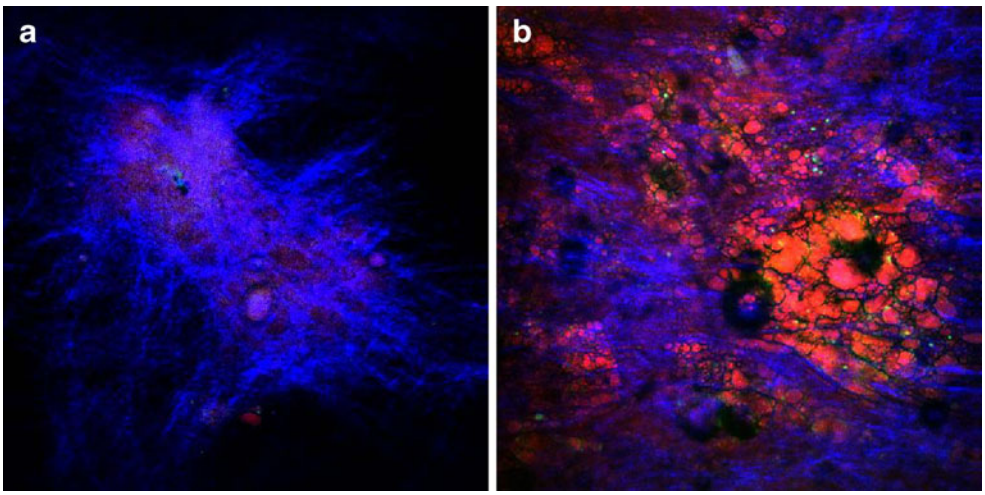

Fig. 8 Epi-NLO images of an advanced plaque obtained at approx. depths of 10 μm (**a**) and 60 μm (**b**) from the lumen surface. *Blue* SHG fibrillar collagen type-I, *red/orange* CARS lipid-rich structure buried under a fibrous cap

information extracted from NLOM images needs to be translated into relevant quantitative data to fully exploit the wealth of information stored in the NLOM images. Sophisticated image analysis methodologies are therefore needed.

Although a wide range of imaging quantification and analysis methods are available, their utility in NLOM still largely remains unexplored. In the context of characterizing atherosclerotic progression, Lilledahl et al. (2007) were the first to use a measure of the SHG: TPEF ratio derived from a pixel-density based image quantification to detect atherosclerosis plaques with reasonable sensitivity and specificity. In another study, Doras et al. (2011) performed multiphoton image reconstruction and also analyzed the change in optical polarization that occurs in atherosclerotic plaque development. Using multimodal CARS imaging, Wang et al. (2009) reported area percentage calculations of collagen and lipid content in the thickened initima of different types of atherosclerosis lesions. These authors were the first to demonstrate that this type of quantification correlates well with histology studies. Secondly, the data showed that Type IV lesions contain the highest lipid concentration, even compared to Type V and VI lesions, possibly implying a regression of lipid accumulation and higher concentrations of fibrous deposits in Type V and VI lesions.

Strupler et al. (2007, 2008) recently conducted two NLOM studies to investigate the three-dimensional heterogeneous accumulation of fibrillar collagen during fibrotic pathologies. In these works Strupler et al. (2007) concluded that their protocol could be applied to analyze other types of diseased tissues, such as tissue from the cardiovascular system; however, according to Mostaço-Guidolin et al. (2010), Strupler's protocol is not optimal to track extracellular changes associated with atherosclerotic lesion progression. Mostaço-Guidolin et al. (2010) proposed a numerical optical index for determining plaque burden based on a linear combination of the three phenomenological scores originally proposed by Strupler et al. (2007) which also included terms to account for the strong intercorrelation among major extracellular components during plaque progression.

The q quantitative evaluation of some texture descriptors of atherosclerotic lesions has also been reported (Mostaço-Guidolin et al. 2011). Textural features extracted from NLOM images were investigated for their utility in providing quantitative descriptors of structural and compositional changes associated with plaque development. Notably, many of these tonal-textural parameters showed different depth profiles in the NLO signals obtained from younger and older rabbit arteries. Some of the tonal-texture parameters could be directly attributed to the different composition and structures of the lesions.

Conclusion

NLOM has demonstrated its un-doubted strength in arterial tissue imaging by providing unprecedented high-resolution biochemical maps of tissue composition on both the axial and the lateral dimensions without added stains. Its specific advantage of being able to image deeply into intact tissue enables researchers for the first time to look at the bulk tissue biology without chemical or physical perturbation. While more NLOM studies on arterial imaging will certainly emerge as the technology becomes more affordable and robust, we believe that the focus should gradually shift from proof-of-concept toward developing standards of image quantification and interpretation in order to realize the full potential of NLOM as a diagnostic tool.

Conflicts of interest None.

References

Barad Y, Eisenberg H, Horowitz M, Silberberg Y (1997) Nonlinear scanning laser microscopy by third harmonic generation. Appl Phys Lett 70(8):922–924

Barlis P, Schmitt JM (2009) Current and future developments in intracoronary optical coherence tomography imaging. EuroIntervention 4(4):529–533

Barlis P, Serruys PW, Devries A, Regar E (2008a) Optical coherence tomography assessment of vulnerable plaque rupture: predilection for the plaque 'shoulder'. Eur Heart J 29(16):2023

Barlis P, Ferrante G, Del Furia F, Di Mario C (2008b) In-vivo characterisation of coronary atherosclerosis with optical coherence tomography. Med J Aust 188(12):728

Boulesteix T, Pena AM, Pages N, Godeau G, Sauviat MP, Beaurepaire E, Schanne-Klein MC (2005) Micrometer scale ex vivo multiphoton imaging of unstained arterial wall structure. Cytometry A 69A:20–26

Delaney P, Harris M (2006) Fiber-optics in scanning optical microscopy. In: Pawley JB (ed) Handbook of biological confocal microscopy, 3rd edn. Springer, New York, pp 501–515

Denk W, Strickler JH, Webb WW (1990) Two-photon laser scanning fluorescence microscopy. Science 248(4951):73–76

Doras C, Taupier G, Barsella A, Mager L, Boeglin A, Bulou H, Bousquet P, Dorkenoo KD (2011) Polarization state studies in second harmonic generation signals to trace atherosclerosis lesions. Opt Express 19:15062–15068

Dudovich N, Oron D, Silberberg Y (2002) Single-pulse coherently controlled nonlinear Raman spectroscopy and microscopy. Nature 418:512–514

Duncan MD, Reintjes J, Manuccia TJ (1982) Scanning coherent anti-Stokes Raman microscope. Opt Lett 7(8):350–352

Freudiger CW, Min W, Saar BG, Lu S, Holtom GR, He C, Tsai JC, Kang JX, Xie XS (2008) Label-free biomedical imaging with high sensitivity by stimulated Raman scattering microscopy. Science 322:1857–1861

Ganikhanov F, Carrasco S, Xie XS, Katz M, Seitz W, Kopf D (2006) Broadly tunable dual-wavelength light source for coherent anti-Stokes Raman scattering microscopy. Opt Lett 31:1292–1294

Hansson GK (2005) Inflammation, atherosclerosis, and coronary artery disease. N Engl J Med 352(16):1685–1695

Hodgson JM, Reddy KG, Suneja R, Nair RN, Lesnefsky EJ, Sheehan HM (1993) Intracoronary ultrasound imaging: correlation of plaque morphology with angiography, clinical syndrome and procedural results in patients undergoing coronary angioplasty. J Am Coll Cardiol 21(1):35–44

Jang IK, Tearney GJ, MacNeill B, Takano M, Moselewski F, Iftima N, Shishkov M, Houser ST, Aretz H, Halpern EF, Bouma BE (2005) In vivo characterization of coronary atherosclerotic plaque by use of optical coherence tomography. Circulation 111(12):1551–1555

Jo JA, Fang Q, Papaioannou T, Baker JD, Dorafshar AH, Reil T, Qiao JH, Fishbein MC, Freischlag JA, Marcu L (2006) Laguerre-based method for analysis of time-resolved fluorescence data: Application to in-vivo characterization and diagnosis of atherosclerotic lesions. J Biomed Opt 11(2):021004

Kim S-H, Lee E-S, Lee JY, Lee ES, Lee BS, Park JE, Moon DW (2010) Multiplex coherent anti-stokes raman spectroscopy images intact atheromatous lesions and concomitantly identifies distinct chemical profiles of atherosclerotic lipids. Circ Res 106:1332–1341

Ko ACT, Ridsdale A, Smith MSD, Mostaço-Guidolin LB, Hewko MD, Pegoraro AF, Kohlenberg EK, Schattka B, Shiomi M, Stolow A, Sowa MG (2010) Multimodal nonlinear optical imaging of atherosclerotic plaque development in myocardial infarction-prone rabbits. J Biomed Opt 15(2):020501

Le TT, Langohr IM, Locker MJ, Sturek M, Cheng J-X (2007) Label-free molecular imaging of atherosclerotic lesions using multimodal nonlinear optical microscopy. J Biomed Opt 12(5):054007

Lee JY, Kim SH, Moon DV, Lee ES (2009) Three-color multiplex CARS for fast imaging and microspectroscopy in the entire CH stretching vibrational region. Opt Express 17(25):22281

Libby P (2006) Atherosclerosis: disease biology affecting the coronary vasculature. Am J Cardiol 98(12):S3–S9

Lilledahl MB, Haugen OA, Davies de Lange C, Svaasand LO (2007) Characterization of vulnerable plaques by multiphoton microscopy. J Biomed Opt 12(4):044005

Maffia P, Zinselmeyer BH, Ialenti A, Kennedy S, Baker AH, McInnes IB, Brewer JM, Garside P (2007) Into apolipoprotein-E–deficient mouse carotid artery multiphoton microscopy for 3-dimensional imaging of lymphocyte recruitment. Circulation 115:e326–e328

Major A, Sandkuijl D, Barzda V (2009) Efficient frequency doubling of a femtosecond Yb:KGW laser in a BiB_3O_6 crystal. Opt Express 17:12039–12042

Marcu L, Jo JA, Fang Q, Papaioannou T, Reil T, Qiao JH, Baker JD, Freischlag JA, Fishbein MC (2009) Detection of rupture-prone atherosclerotic plaques by time-resolved laser-induced fluorescence spectroscopy. Atherosclerosis 204(1):156–164

Megens RTA, Reitsma S, Schiffers PHM, Hilgers RHP, De Mey JGR, Slaaf DW, Oude Egbrink MGA, van Zandvoort MAMJ (2007) Two-photon microscopy of vital murine elastic and muscular arteries. J Vasc A 24(5):1337–1348

Megens RTA, oude Egbrink MGA et al (2008) Two-photon microscopy on vital carotid arteries: imaging the relationship between collagen and inflammatory cells in atherosclerotic plaques. J Biomed Opt 13(04):044022

Millard AC, Wiseman PW, Fittinghoff DN, Wilson KR, Squier JA, Müller M (1999) Third-harmonic generation microscopy by use of a compact, femtosecond fiber laser source. Appl Opt 38 (36):7393–7397

Miyata K, Rotermund F, Petrov V (2009) Efficient frequency doubling of a low-power femtosecond Er-fiber laser in BiB_3O_6. IEEE Photo Technol Lett 21(19):1417–1419

Mizutani G, Koyama T, Tomizawa S, Sano H (2005) Distinction between some saccharides in scattered optical sum frequency intensity images. Spectrochim Acta A Mol Biomol Spectrosc 62 (4–5):845–849

Mostaço-Guidolin LB, Sowa MG, Ridsdale A, Pegoraro AF, Smith MSD, Hewko MD, Kohlenberg EK, Schattka B, Shiomi M, Stolow A, Ko ACT (2010) Differentiating atherosclerotic plaque burden in arterial tissues using femtosecond CARS-based multimodal nonlinear optical imaging. Biomed Opt Express 1:59–73

Mostaço-Guidolin LB, Ko AC-T, Popescu DP, Smith MSD, Kohlenberg EK, Shiomi M, Major A, Sowa MG (2011) Evaluation of texture parameters for the quantitative description of multimodal nonlinear optical images from atherosclerotic rabbit arteries. Phys Med Biol 56:5319. doi:10.1088/0031-9155/56/16/016

Murugkar S, Brideau C, Ridsdale A, Naji M, Stys PK, Anis H (2007) Coherent anti-Stokes Raman scattering microscopy using photonic crystal fiber with two closely lying zero dispersion wavelengths. Opt Express 15:14028–14037

Naghavi M, Libby P, Falk E et al (2003) Review: current perspective: from vulnerable plaque to vulnerable patient: a call for new definitions and risk assessment strategies: Part I. Circulation 108:1664–1672. doi:10.1161/01.CIR.0000087480.94275.97

Parasassi T, Yu W, Durbin D, Kuriashkina L, Gratton E, Maeda N, Ursini F (2000) Two-photon microscopy of aorta fibers shows proteolysis induced by LDL hydroperoxides. Free Radic Biol Med 28:1589–1597

Paulsen HN, Hilligse KM, Thøgersen J, Keiding SR, Larsen JJ (2003) Coherent anti-Stokes Raman scattering microscopy with a photonic crystal fiber based light source. Opt Lett 28:1123–1125

Pegoraro AF, Ridsdale A, Moffatt DJ, Jia Y, Pezacki JP, Stolow A (2009a) Optimally chirped multimodal CARS microscopy based on a single Ti:sapphire oscillator. Opt Express 17:2984–2996

Pegoraro AF, Ridsdale A, Moffatt DJ, Pezacki JP, Thomas BK, Fu L, Dong L, Fermann ME, Stolow A (2009b) All-fiber CARS microscopy of live cells. Opt Express 17(23):20700–20706

Phipps J, Sun Y, Saroufeem R, Hatami N, Marcu L (2009) Fluorescence lifetime imaging microscopy for the characterization of atherosclerotic plaques. Proc Soc Photo Opt Instrum Eng 7161:71612G

Prent N, Green C, Greenhalgh C, Cisek R, Major A, Stewart B, Barzda V (2008) Inter-myofilament dynamics of myocytes revealed by second harmonic generation microscopy. J Biomed Opt 13 (4):041318–1–041318–7

Rinia HA, Burger KNJ, Bonn M, Müller M (2008) Quantitative label-free imaging of lipid composition and packing of individual cellular lipid droplets using multiplex CARS microscopy. Biophys J 95(10):4908–4914

Schenke-Layland K, König K, Riemann I, Stock UA (2005) Imaging of cardiovascular structures using near-infrared femtosecond multiphoton laser scanning microscopy. J Biomed Opt 10:024017. doi:10.1117/1.1896966

Schenke-Layland K, Madershahian N, Riemann I, Starcher B, Halbhuber KJ, König K, Stock UA (2006) Impact of cryopreservation on extracellular matrix structures of heart valve leaflets. Ann Thorac Surg 81(3):918–926

Sheppard CJR, Gannaway JN, Kompfner R, Walsh D (1977) Scanning harmonic optical microscope. IEEE J Q Electron 13(9):100D

Smith MSD, Ko ACT, Ridsdale A, Schattka B, Pegoraro A, Hewko MD, Shiomi M, Stolow A, Sowa MG (2009) A single-photon fluorescence and multi-photon spectroscopic study of atherosclerotic lesions. Proc SPIE 7386:73860I

Spence DE, Kean PN, Sibbett W (1991) 60-fsec pulse generation from a self-mode-locked Ti:sapphire laser. Opt Lett 16(1):42–44

Strupler M, Pena AM, Hernest M, Tharaux PL, Martin JL, Beaurepaire E, Schanne-Klein MC (2007) Second harmonic imaging and scoring of collagen in fibrotic tissues. Opt Express 15(7):4054–4065

Strupler M, Hernest M, Fligny C, Martin J-L, Tharaux P-L, Schanne-Klein MC (2008) Second harmonic microscopy to quantify renal interstitial fibrosis and arterial remodeling. J Biomed Opt 13 (5):054041

Sun J, Zhang Z, Lu B, Yu W, Yang Y, Zhou Y, Wang Y, Fan Z (2008) Identification and quantification of coronary atherosclerotic

plaques: a comparison of 64-MDCT and intravascular ultrasound. Am J Roentgenol 190(3):748–754

Suhling K, French PM, Phillips D (2005) Time-resolved fluorescence microscopy. Photochem Photobiol Sci 4(1):13–22

Timmins LH, Wu Q, Yeh AT, Moore JE Jr, Greenwald SE (2010) Structural inhomogeneity and fiber orientation in the inner arterial media. Am J Physiol Heart Circ Physiol 298:H1537–H1545

Thomas P, Pande P, Clubb F, Adame J, Jo JA (2010) Biochemical imaging of human atherosclerotic plaques with fluorescence lifetime angioscopy. Photochem Photobiol 86:727–731

Van Zandvoort M, Engels W, Douma K, Beckers L, Oude Egbrink M, Daemen M, Slaaf DW (2004) Two-photon microscopy for imaging of the (atherosclerotic) vascular wall: a proof of concept study. J Vasc Res 41(1):54–63

Yock PG, Fitzgerald PJ (1998) Optimal directional coronary atherectomy final results of the Optimal Atherectomy Restenosis Study (OARS). Am J Cardiol 81:27E–32E

Yu W, Braz JC, Dutton AM, Prusakov P, Rekhter M (2007) In vivo imaging of atherosclerotic plaques in apolipoprotein E deficient mice using nonlinear microscopy. J Biomed Opt 12 (5):054008

Wang H-W, Langohr IM, Sturek M, Cheng J-X (2009) Imaging and quantitative analysis of atherosclerotic lesions by CARS-based multimodal nonlinear optical microscopy. Arterioscler Thromb Vasc Biol 29(9):1342–1348

Wang H-W, Simianu V, Locker MJ, Cheng J-X, Sturek M (2011) Stent-induced coronary artery stenosis characterized by multimodal nonlinear optical microscopy. J Biomed Opt 16(2):021110

Zoumi A, Lu XA, Kassab GS, Tromberg BJ (2004) Imaging coronary artery microstructure using second-harmonic and two-photon fluorescence microscopy. Biophys J 87:2778–2786

Zumbusch A, Holtom GR, Xie XS (1999) Three-dimensional vibrational imaging by coherent anti-Stokes Raman scattering. Phys Rev Lett 82(20):4142–4145